Materials Today Communications 34 (2023) 104990

Contents lists available at ScienceDirect

Materials Today Communications

journal homepage: www.elsevier.com/locate/mtcomm

Effect of post-drawing and tension on enzymatic degradation of electrospun polycaprolactone nanofibers

David A. Brennan [a], Matthew D. Flamini [a], Jared Posselt [b], Christopher T. Wagner [b], Vince Beachley [a,*]

[a] Department of Biomedical Engineering, Rowan University, Glassboro, NJ 08028, United States
[b] Department of Biomedical Engineering, The College of New Jersey, Ewing, NJ 08628, United States

ARTICLE INFO

Keywords:
Degradation
Nanofiber
Electrospinning
Polycaprolactone
Post draw

ABSTRACT

Electrospun polycaprolactone nanofibers were enzymatically degraded to evaluate the effect of post-draw processing and tension on the rate of degradation. Electrospun polycaprolactone (PCL) nanofibers were drawn to increasing lengths, then submerged in pseudomonas lipase (PS Lipase) solution for a 7-day period. The degradation process and extent of deterioration were evaluated by changes in mass, tensile strength, percent crystallinity, molecular weight, and macromolecular chain alignment on day 0, 3, and 7. The rate of degradation was dependent on the percent crystallinity of the fiber and the degree of alignment in crystalline and amorphous portions of the fiber. Post-drawn PCL fibers maintained mass and tensile strength over 7 days in PS Lipase, while undrawn fibers, degraded within 1 day. Pretension in fibers before enzymatic incubation was critical to maintain the macromolecular structure and tensile strength over the degradation period. Loss of mass and mechanical strength without molecular weight reduction indicated that degradation occured via surface erosion of the material over time rather than enzyme penetration and bulk degradation. Measurement of crystallinity and chain alignment illustrated the effect of automated track drawing on the progression of crystal growth and chain alignment, as well as the changes in macromolecular structure which occurred during the multi-day degradation period.

1. Introduction

Electrospinning is a manufacturing method which has received considerable interest for its ability to produce nanofibers from a range of polymers in a relatively simple and inexpensive process [1–3]. Applications for electrospun nanofibers range from textiles to composite reinforcement, to tissue engineering [2,4,5]. In many applications, a suitable rate of degradation and maintenance of mechanical strength is a critical material property [6].

Polycaprolactone (PCL) has been studied for a wide range of applications as it is biocompatible, resorbable in the body, and is biodegradable in the environment. Degradation of PCL primarily occurs through hydrolysis of the ester bonds, which is catalyzed by enzymes secreted by cells and microorganisms [7–12]. Degradation of polymers generally initiates in the polymer amorphous regions and can occur as bulk degradation or surface erosion. The degradation path and rate is highly dependent on the rate of penetration of degradation media into the material [7,13]. It has been observed that even in the absence of enzyme or other chemical reactions, surrounding media can deteriorate polymers if it can penetrate into the bulk material, disturbing the interior macromolecular structures and initiating hydrolysis [14]. The loosely packed structure of the amorphous regions, comprised of randomly coiled unaligned chains, are more susceptible to penetration compared to densely packed crystalline regions. Thus, in the amorphous region, more bonds susceptible to lysis are exposed to any catalyzing enzymes present in the surrounding media [8,15,16]. PCL degradation by lipase has been shown to vary greatly with sample processing, where films degrade at much slower rates than microparticles, and microfiber degradation varies with draw ratio [8,9,12,17]. However, there is little information on the degradation rate of electrospun PCL nanofibers and the effect of draw ratio and tension on this process. It is critical to understand these mechanisms when engineering PCL nanofiber structures with load bearing requirements, such as orthopedic implants.

Previously, post-drawing was used to enhance the tensile strength of

* Corresponding author.
E-mail address: beachley@rowan.edu (V. Beachley).

https://doi.org/10.1016/j.mtcomm.2022.104990
Received 25 August 2022; Received in revised form 21 October 2022; Accepted 21 November 2022
Available online 24 November 2022

electrospun polycaprolactone by aligning and extending polymer chains in the nanofiber [18]. The following experiments analyzed the effects of post-drawing induced polymer chain alignment on the degradation rate of PCL nanofiber bundles. It was hypothesized that an inverse relation exists between fiber draw ratio during collection and rate of enzymatic degradation (Fig. 1). Drawn fibers, with aligned, extended chains, and increased crystallinity will have densely compacted macromolecular structures. These structures will prevent enzyme penetration into the polymer fiber and limit enzyme cleavage of ester bonds on the fiber surface, initially protecting deeper ester bonds within the fiber. Thus, post-drawing was expected to reduce fiber degradation rate and improve retention of mechanical integrity over time. In comparison, undrawn fibers, with unorganized polymer chains and larger amorphous regions; will have loosely packed macromolecular structures. These chain formations will be susceptible to enzyme penetration allowing degradation of ester bonds more readily. The amorphous chain structures will degrade at an increased rate and lose mechanical strength more quickly over time. Based on the reported long degradation times for bulk PCL in the body (6 months – 4 years), we expect that both drawn and undrawn fibers will experience minimal loss of mass, crystallinity, and mechanical strength, when submerged in PBS with no enzyme to catalyze hydrolysis [7].

2. Methods and materials

2.1. Electrospinning

Electrospinning was completed using a solution of 18 % wt./vol. PCL (Mn 80,000 Sigma Aldrich) in 3:1 dichloromethane (DCM) and dimethylformamide (DMF). In all samples, electrospinning was completed using a voltage of 10 kV, applied to a 21-gauge needle positioned 10 cm above the automated tracks. The polymer solution was loaded into a 5 ml polypropylene syringe, with the syringe pump (New Era Pump Systems) set to 1 ml/hr. Electrospinning was completed at ambient temperatures (25 °C), with the relative humidity maintained between 45 % and 55 %.

Samples of electrospun fibers were collected under 5 different conditions while maintaining solution and spinning parameters described above. Undrawn, randomly aligned fibers were collected onto a flat plate with no further processing. Aligned fiber samples were collected using an automated-track system in order to collect fibers at increasing draw ratios (Fig. 1) ($DR = Length_{Final}/Length_{Initial}$) [18]. Fibers were deposited across the parallel tracks with a gap of 6 cm and collected without post-drawing at DR1; or post-drawn up to a max of 24 cm at DR4. Track speed was adjusted to draw each at a linear extension rate of 1 mm/s for all draw ratios.

After collection, sheets of fibers were cut into strips, rolled into bundles, and the mass, fiber diameter, molecular weight, and mechanical strength were evaluated at day 0, 3, and 7 (D0, D3, D7). Mass loss data was collected by weighing a unique sample at days 0, 3, and 7. Mechanical strength and molecular weight tests are sacrificial and cannot be tested further, requiring a unique replicate sample for evaluation at each time point. All fiber samples were tied to 3D printed frames using a surgeon's square knot, submerged in solution, then retrieved and tested. Day 0 samples were submerged for 5 min so that testing conditions were similar to samples removed on day 3 and day 7. The frame ensured samples had the same gauge length (2 cm) and allowed fiber bundles to be tied in tension. One end of a fiber bundle was first secured to a frame post using a surgical knot [19]. The bundle was pulled taught by hand with the minimum tension required to ensure there was no slack in the sample when tied to the second frame post using the same method (Supplemental Fig. 1).

In addition, the effect of pretension on strength retention and enzyme penetration during degradation was observed. To pretension samples, the fiber bundles were tied to a frame with a sliding fixture attached by a screw on one end. After the samples were secured by a surgeon knot, as above, a weight was tied to the sliding fixture to tension the bundle (Supplemental Fig. 1). Samples were preloaded to 7 % and 15 % of the average load per linear density (N/(mg/cm)) at failure, measured on D0. The exact weight applied changed slightly based on the weight of the sample. Values of 7 % and 15 % load at failure were selected based on the load applied in ACL surgery clinical practice [20]. After 5 min under load, the screw was tightened to immobilize the fibers in place, maintaining tension after the weight was removed and throughout the degradation period. Samples of each draw ratio (DR1, 2, 3, 4) were prepared in this manner and submerged in lipase solution for 7 days. After observing that pretension had the greatest effect on DR1 strength, samples of DR1 fibers (n = 3) were pretensioned to a moderate (7 % max load) and overload (15 % max load) before submersion in both PBS and lipase solutions [20].

2.2. Enzymatic degradation

Samples were submerged in degradation solutions of phosphate buffered saline (PBS) or PBS containing 0.12 mg/ml pseudomonas lipase (PS Lipase, Sigma Aldrich) at 37 °C up to 7 days. PS lipase and concentration were chosen based on a review of published literature illustrating the enzyme's ability to catalyze hydrolysis of PCL ester bonds as

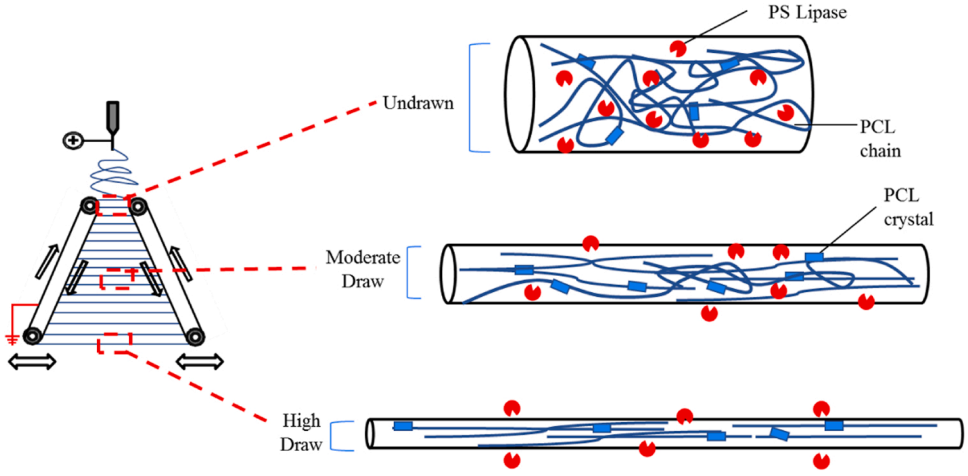

Fig. 1. (Left). Automated-tracks facilitate continuous collection and post-drawing of individual PCL nanofibers. (Right) As the fibers are post-drawn, the diameter decreases as polymer chains align to the axis and compact together. Undrawn fibers with unaligned chains possess larger spaces between chains allowing enzyme to more readily penetrate compared to drawn fibers with aligned polymer chains, compacted together.

well as a preliminary test of different lipase concentrations [11,12]. In the preliminary test 0.05 mg/ml caused little to no degradation; in comparison, at concentrations of 0.5 mg/ml, all fiber samples degraded at a rate which prevented sample retrieval for analysis (Supplemental Fig. 2). Samples were removed from solution for analysis after 3 days (D3) and 7 days (D7). After removal from solution, samples were washed for 10 min using deionized water in an ultrasonic bath followed by a rinse under a stream a deionized water. This process was completed 3 times to remove active enzyme and dissolved salts from samples before testing. After cleaning, samples used for determining changes in mass loss, crystallinity, morphology, and molecular weight were dried under vacuum for 24 h. before analysis. Fiber bundles used for tensile tests were kept submerged in deionized water after cleaning, to prevent stress concentrations caused by shrinking after drying.

2.3. Mass loss

A balance (Mettler Toledo) with a precision of 0.01 mg was used to weigh samples before and after degradation. Each sample was weighed at D0 before submersion and after removal on D3 or D7 after drying under vacuum for 24hrs. For each sample type, the entire set was weighed three times in rotation to minimize weighing errors. The percentage of mass loss was determined by comparing the final mass (m_{Final}) after a degradation period with the initial mass ($m_{Initial}$) recorded at collection. Percent mass loss was calculated as: % Mass Loss = $((m_{Initial} - m_{Final})/m_{Initial}) \times 100$. After weights were recorded, dried samples were used to determine changes in morphology, percent crystallinity, and molecular weight at D3 or D7.

2.4. Morphology

A portion of the dried sample was cut and further prepared for imaging. A Scanning Electron Microscope (SEM, Phenom Pure) was used to capture images of the fibers before and after submersion in degradation media. At each time point, 3 images were taken at magnification 800 × and 8000 × (n = 6 total) to view gross bundle morphology as well as individual fiber diameter. Photos were analyzed using Image J software. Images taken at D0 were used to measure initial fiber diameter, surface texture and morphology.

2.5. Molecular weight

Gel permeation chromatography (GPC) was used to determine changes in the polymer weight average molecular weight (MW_w) of the samples during the degradation period. Before analysis, samples were washed using the same method outlined in 6.2.2. The washed PCL samples were prepared in HPLC-grade Tetrahydrofuran (THF, Fisher Scientific) at 1 mg/ml before filtration through 0.45 mm PTFE membranes. Filtered samples (30 ml) were injected for separation (Alliance e2695 module, Waters Corporation, Milford, MA) using THF isocratic carrier at 1 ml/min. Separation occurred across two columns (HSPgel RT MB-L 3 mm, MW100–10,000 followed by HSPgel HT MB-H 5 mm, MW5K-10 M) prior to refractive index detection (2414 RI detector, Waters Corporation, Milford, MA). MW_w was calculated against a 12-point polystyrene standard calibration. Samples are assessed at D0, D3 and D7 after exposure to PBS and enzyme solutions.

Observations of the molecular weight were used to determine if the fibers degrade via surface erosion or bulk degradation. Surface erosion occurs when degradation media's inability to penetrate the polymer results in degradation at the surface alone [7]. During this process, bond scission occurs and chain fragments diffuse into the supernatant and do not appear in GPC analysis. Conversely, bulk degradation would occur if the degradation media can penetrate that polymer bulk and cause hydrolysis throughout the materials volume, and results in reduction of molecular weight over time.

2.6. Mechanical strength

Fiber bundles were tested in uniaxial tension at a strain rate of 5 mm/min using a Shimadzu EZ-SX with a 100 Newton load cell on day 0, 3, and 7. The strain rate was chosen to avoid brittle behavior caused by high rates of strain, while completing the test in under 30 s as prescribed by ASTM standards for polymer fiber tensile tests [21]. Fiber bundles were removed from 3D printed frames without untying by carefully sliding the loop off its supporting post. An S-hook was then carefully threaded through the previously tied loops. S-hooks were used to prevent stress concentrations from clamps.

At D0 fiber bundles were soaked in PBS for 5 min at 37C and subsequently washed as described in Section 2.2. At D3 and D7 samples exposed to PBS and PS Lipase were removed, washed as described in Section 2.2, and tested without drying. Samples for mechanical testing are destroyed by testing and cannot be returned to the degradation media. Remnants of tensile tested specimens were retrieved and dried to measure mass loss and then molecular weight.

Ultimate tensile strength was calculated from the maximum recorded load divided by the bundle cross sectional area. Young's modulus was calculated from the linear portion in the initial slope of the stress-strain curves. Strain was calculated as the total change in length at failure divided by initial length (20 mm). The specific strength was calculated as the recorded load (N) divided by the linear density of the sample (kg/m). The cross-sectional area was calculated as the linear density divided by the known bulk density (1.145 g/cm^3). The axial stiffness was calculated as the force (N) divided by the displacement (m) of the nanofiber bundle at 10 % strain.

2.7. Percent crystallinity and orientation morphology

The absorption spectra of PCL fibers of each draw ratio were measured at D0, D3, and D7 (n = 5) using polarized and unpolarized Fourier-transform infrared spectroscopy (FTIR) (Thermo, iS50 Nicolet). In unpolarized spectra, the carbonyl vibration band at 1727 cm^{-1} was resolved into crystalline (1725 cm^{-1}) and amorphous (1736 cm^{-1}) regions as described by He et al. [22]. The absorption intensities of these regions were used to calculate percent crystallinity as: $X_C = A_c/(A_c + \gamma A_a)$ where A_c was the crystalline region intensity, A_a was the amorphous region intensity, and γ was the absorption coefficient for PCL ($\gamma = 1.46$).

A polarizing filter was used to control the vibrational direction of the FTIR beam contacting the sample. The direction of polarization was defined as parallel ($A^{\parallel}$) when the beam vibration direction was the same as the fiber axis and perpendicular ($A^{\perp}$) when it was normal to the fiber axis. Polarized spectra were used to evaluate polymer chain alignment to the fiber axis by calculating dichroic ratio of the peaks at 1293 cm^{-1} and 1157 cm^{-1}. Because these peaks are both associated with the C-C and C-O bond of the PCL backbone chain in the crystalline (1293 cm^{-1}) and amorphous (1157 cm^{-1}) phases; the ratio of the parallel ($A^{\parallel}$) and perpendicular($A^{\perp}$) absorption peaks describes the alignment of the polymer chain to the fiber axis [23–25]. Dichroic ratios > 1 indicate an anisotropic material with chain orientation favoring the fiber axis, while value < 1 indicate anisotropic structure with backbone favoring alignment normal to the fiber axis. Dichroic ratios of 1 indicate an isotropic material with even distribution of chains parallel and perpendicular to the axis.

3. Results and discussion

3.1. Electrospinning

The system produced aligned arrays of nanofibers stretched from 6 up to 24 cm during collection (4x initial length). Fibers were collected across the initial gap of the automated tracks and stretched to a final length at the collection tray (Fig. 1). The geometry of the tracksand the

draw ratio of the fibers can be adjusted; which allows the drawing of thousands of individual fibers per minute to a predetermined draw ratio. As the fibers are drawn to their final length, they are sheared from the tracks by a stationary collection tray located between the tracks [18]. The fibers adhere to the collection tray at opposite ends , maintaining tension in the sample post-collection. The design of the automated tracks successfully integrates electrospinning with the post-drawing process utilized in conventional fiber manufacture. The major highlights of this design are the ability to spin and post-draw individual fibers before collection into a mesh, simultaneously processing of thousands of fibers in a continuous automated process.

3.2. Morphology

The effect of draw ratio during fiber spinning and collection on PCL fiber morphology was evaluated using SEM images. Supplemental Fig. 3 shows that the automated-track system produced aligned arrays of smooth fibers with uniform diameters upon spinning and drawing. The average fiber diameter of undrawn fibers was 716 nm and reduced to 509 nm at a draw ratio of 4 (Supplemental Fig. 3). The reduction of fiber diameter from DR1 to DR2, closely follows the reduction predicted by the conservation of volume equation ($L_1 * \pi * r_1^2 = L_2 * \pi * r_2^2$). The measured diameter of DR3 and DR4 are 120 nm and 151 nm larger than predicted by conservation of volume. Larger than predicted diameters may be caused by partial relaxation of the fibers to pre-drawing dimensions when tension was removed during preparation for imaging [26]. This occurs because the low glass transition temperature (Tg) of PCL (− 60 °C) allows chain motion at ambient temperature (25 °C). In higher draw ratio samples, extended chains have a greater distance available to retract, which could cause a more pronounced effect. Necking was not observed in SEM images of the drawn fibers.

3.3. Mass loss

Over a seven-day period, samples were removed from degradation solution, washed, dried, and weighed to evaluate mass loss during exposure to solutions of PBS and PS lipase. In PBS, all samples retained greater than 95 % of their total weight over seven days (Supplemental Table 1). These changes of less than 5 % mass are possibly due to changes in humidity effecting the scale on the day of weighing. Under exposure to 0.12 mg/ml enzyme solution, undrawn, randomly aligned (RND) and undrawn aligned fibers (DR1) degraded completely by day 2 and were impossible to retrieve for testing. All drawn fibers (DR2, DR3, DR4) survived enzymatic degradation over the 7-day period (Supplemental Table 1). At D3 all DR2, DR3, and DR4 samples lost approximately 17 % of their total weight. At D7 mass loss was the lowest in DR2 (− 25 %), highest in DR3 (− 35 %), and mid-range in DR4 (− 29 %). Despite lower draw ratio and lower total crystallinity, DR2 retained the most mass. This was contrary to results seen in melt spun microfibers, which were drawn to increasing ratios while maintaining the same final diameter between samples. In that study, total crystallinity consistently increased with draw ratio and degradation rate consistently slowed as draw ratio and crystallinity was increased [8]. Comparing the results between these studies indicates that degradation rate is dependent on the alignment and compaction of the amorphous and crystalline regions as well as the total crystallinity. In the presented work, greater mass loss in DR4 (− 29 %) compared to DR2 (− 25 %) possibly occurs as a result of higher extension of amorphous chains and increased surface area to volume ratio in the smaller diameter DR4 fibers. Although drawing forms densely packed crystal and amorphous regions, it also results in higher extension of amorphous chains at the fiber surface. Highly extended chains will result in increased exposure of ester bonds at the fiber surface.

Comparing the pretensioned and untensioned DR1 samples which both possess the same initial crystallinity; only the pretensioned sample survived the 7-day degradation period. Survival of the pretension sample indicates that pretension acted as a secondary drawing stage which further increases alignment and compaction of polymer chains, reducing enzymatic penetration. It is likely that the tension and elevated temperature (37 °C) also promotes new crystal formation during the degradation period, which would compete with the removal of crystals by hydrolysis of polymer ester bonds.

3.4. Molecular weight

GPC shows no large difference in molecular weight between samples at D0, or D7 when exposed to PBS or Lipase (Supplemental Fig. 4). The loss of mass and mechanical strength over time without reduction in molecular weight indicates that degradation proceeds through surface erosion of the polymer fiber. Degradation via surface erosion occurs by hydrolysis of bonds in the polymer backbones at the surface of the material by the enzyme. During this process, bond scission occurs and chain fragments diffuse into the supernatant and would not appear in GPC analysis. In the case of bulk scission, the degraded polymer chains would remain trapped in the bulk and would therefore appear in GPC. This agrees with the established pathways of polymers surface erosion, and results reported for PCL in bulk, films, and fibers [7,27].

3.5. Mechanical strength

Day 0: The automated track drawing process increased tensile strength with increasing draw ratio at D0. Ultimate tensile strength increased by 7.6 times from DR1 to DR4 (Fig. 2). This increase in strength was similar to trends in tensile strength reported for PCL microfibers [8,28,29]. In a similar fashion, Young's modulus increased a total of 7.4 times from DR1 to DR4. In DR4 fiber bundles, the average ultimate tensile strength and Young's modulus were 663 MPa, 1.16 GPa, respectively. For all aligned fibers (DR1, DR2, DR3, DR4), samples failed at a strain of approximately $\sum = 1$ (Supplemental Table 2). Failure at the same elongation between samples indicates load transfer between the fibers, compared to fiber bundles without load transfer which fail at a range of elongations at break [30]. The tensile properties of RND fibers were 7 times lower than DR1 and break elongation occurred at approximately 3 times the initial length. At D0, group to group comparisons of mechanical properties and crystallinity using Mann-Whitney analysis had $p < 0.05$ when highlighted in green in Supplemental Table 3.

Day 3 and 7: All aligned fiber samples submerged in PBS retained 90 % or more of their initial tensile strength properties (Fig. 2). On D7, the ultimate strength and Young's modulus of DR1 increased by 1.4 × and 1.9 ×, respectively. DR4 fibers experienced a similar increase of 1.2 ×, and 1.4 × in ultimate tensile strength and Young's modulus at D7 (Fig. 2). In contrast, random and undrawn aligned fibers in PS lipase degraded fully and were impossible to mechanically test by D3. All drawn samples survived the degradation period, with reductions in tensile strength. At D7 the ultimate tensile strength had decreased by: DR2 = − 75 %, DR3 = − 73 %, and DR4 = − 83 % (Fig. 3). The reduction in Young's modulus at D7 was: DR2 = − 11 %, DR3 = − 63 %, and DR4 = − 29 % (Fig. 3). In Mann-Whitney group to group comparisons of mechanical properties and crystallinity at D0 and D7 had $p < 0.05$ when highlighted in green in Supplemental Table 4.

All DR1 samples pretensioned before submersion in PBS or PS lipase increased in ultimate tensile strength and Young's modulus by D7. When pretensioned to 7 % (of the average load per linear density at failure) and submerged in PBS, DR1 showed an increase in ultimate tensile strength (3.8 ×) and Young's modulus (3.2 ×) (Fig. 4). Samples pretensioned to 15 % (of the average load per linear density at failure) in PBS increased ultimate tensile strength and Young's modulus by 3.1 × and 4.5 ×, respectively (Fig. 4). When submerged in PS lipase and pretensioned to 7 % max load, the sample ultimate tensile strength (2.2 ×) and Young's modulus (2.3x) increased over time, despite the presence of enzyme. Samples loaded to 15 % max load and submerged in

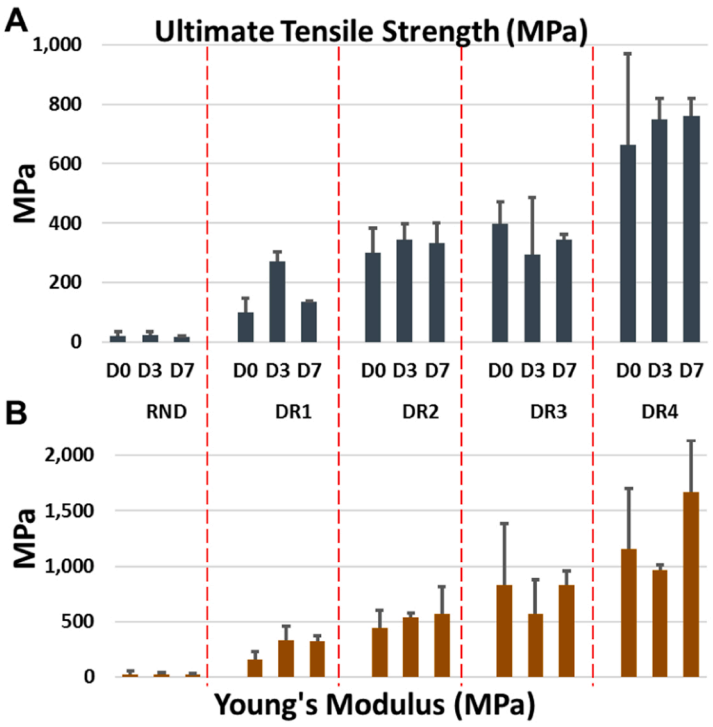

C

% Mass Loss		
	Day 3	Day 7
RND	0.1 ± 0.1	0.2 ± 0.1
DR1	3.0 ± 2.0	1.0 ± 0.6
DR2	3.0 ± 2.0	2.0 ± 1.0
DR3	1.0 ± 1.0	1.3 ± 1.0
DR4	2.4 ± 2.0	1.0 ±0.4

Fig. 2. A.) Changes in ultimate tensile strength, B.) Young's modulus, and C.) mass loss of electrospun PCL nanofibers; collected on a flat plat (RND), and post-drawn to a draw ratio (DR) of 1, 2, 3, 4, over seven days in PBS.

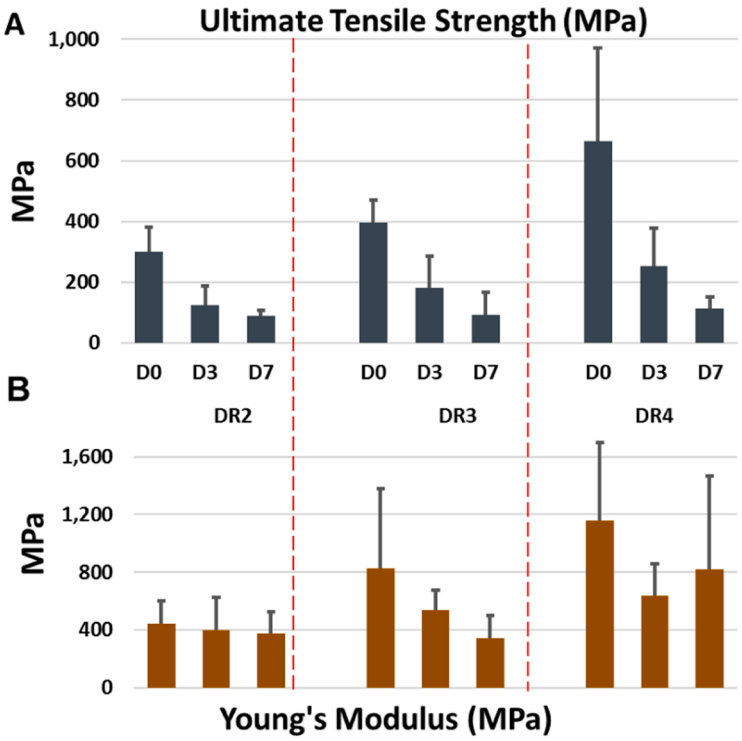

C

% Mass Loss		
	Day 3	Day 7
DR2	17 ± 8	25 ± 5
DR3	18 ± 1	36 ± 2
DR4	17 ± 7	29 ± 11

Fig. 3. A.) Change in ultimate tensile strength, B.) Young's modulus and C.) mass loss of electrospun PCL nanofiber post-drawn to a draw ratio (DR) of 2, 3, and 4, over seven days in PS Lipase.

enzyme solution increased in ultimate tensile strength (1.1 ×) and Young's modulus (1.9 ×) as well. When pretensioned to 7 % and submerged in PBS for 7 days, DR1 samples can achieve approximately 50 % the ultimate tensile strength and Young's modulus of DR4 at D0. The pretensioned DR1 samples were capable of retaining mass for 7 days and increased in tensile strength compared to untensioned DR1 samples which degraded in 2 days and were not possible to mechanically test. These two qualities together indicate that the pretension process acts as a secondary draw stage. This continues to increase chain alignment and compaction, thereby increasing tensile strength and preventing enzyme

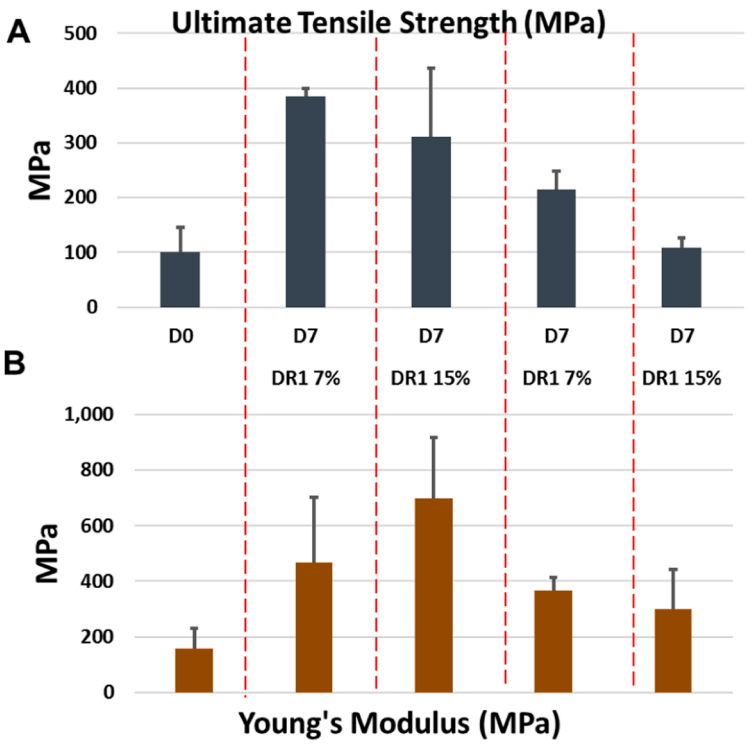

C

% Mass Loss Day 7	
7% Pretension PBS	0.3 ± 0.2
15% Pretension PBS	2.2 ± 1
7% Pretension PS Lipase	32 ± 5
15% Pretension PS Lipase	50 ± 3

Fig. 4. A.) Ultimate tensile strength, B.) Young's modulus, and C.) mass loss of aligned, undrawn (DR1) electrospun PCL nanofibers pretensioned to 7 % and 15 % their maximum load, submerged in PBS and PS Lipase over 7 days.

penetration. Group to group comparisons of mechanical properties and crystallinity at D0 and D7 of pretensioned samples using Mann-Whitney analysis had $p < 0.05$ when highlighted in green in Supplemental Table 5.

3.6. Percent crystallinity and chain alignment

At day 0, 3, and 7 PCL nanofiber crystallinity was calculated by FTIR and curve fitting techniques to resolve the carbonyl band of the spectra into crystalline and amorphous peaks. The Dichroic ratio of the peaks 1157 cm^{-1} and 1293 cm^{-1} (C-C & C-O stretching) in aligned fiber bundles was evaluated to determine alignment of the amorphous and crystalline polymer chains to the fiber axis, respectively. Because the IR beam was focused on multiple fibers in the bundle, it was not possible to determine the Dichroic ratio of fibers in a randomly aligned mesh.

Day 0: RND and DR1 fiber bundles displayed an initial percent crystallinity of 69 % and 74 %, respectively (Fig. 5**A**). This was high in comparison to values reported for PCL undrawn electrospun fiber, undrawn melt fiber, and drawn melt spun fiber crystallinity (40–63 %) [9,31,32]. [23,32]. Total crystallinity initially decreases as draw increases, lowering to 60 % at DR2, and 49 % at DR3. As draw increases to DR4, crystallinity increased to 71 %. The dichroic ratio of the amorphous peak (1157 cm^{-1}) was greater than 1 for all aligned fiber samples, indicating preferential alignment of amorphous chains parallel to the fiber axis. The dichroic ratio of the crystalline peak was greater than 1 for DR2 and DR4, indicating parallel alignment. DR1 and DR3 have ratios of less than one, indicating perpendicular alignment of the crystalline region to the fiber axis. Both the amorphous and crystalline

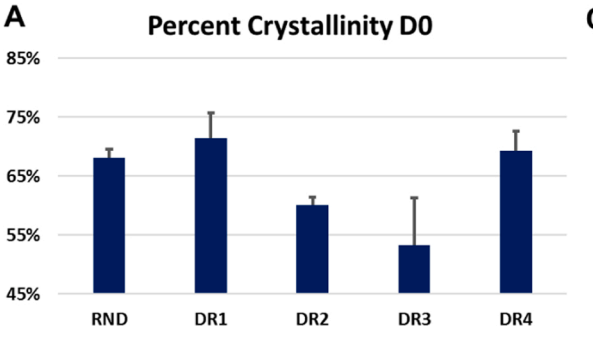

B

Dichroic Ratio (A∥/A⊥)				
	DR1	DR2	DR3	DR4
Amorphous (157cm^{-1})	1.2	3.7	1.8	3.6
Crystalline (1293cm^{-1})	0.8	1.9	0.4	1.2

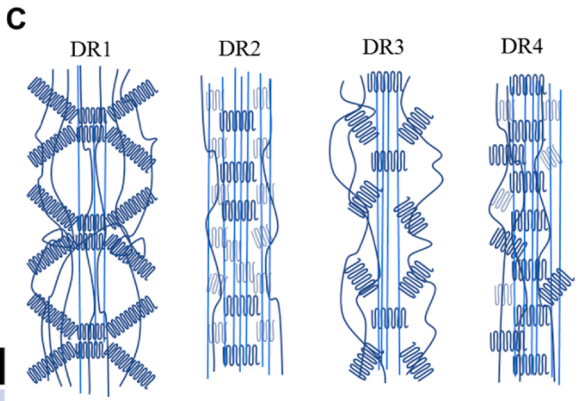

Fig. 5. (A) Changes in percent crystallinity and (B) Dichroic Ratio of the crystalline and amorphous regions with draw ratio at Day 0. C.) Proposed diagram of crystallinity and chain alignment with draw ratio.

dichroic ratio show a similar pattern of values close to 1 at DR1, greater than 1 at DR2, decrease in dichroic ratio at DR3, followed by a second increase at DR4 to values greater than one (Fig. 5**B**).

Comparing the changes in percent crystallinity with the changes in amorphous and crystalline dichroic ratio as draw ratio increases illustrates that crystallization during electrospinning and drawing occurs in stages (Fig. 5**C**). In the first stage, polymer fibers crystallize as spun from the solution, with low chain alignment parallel to the axis of the fiber (DR1). During the initial stages of drawing (DR2, DR3) crystals established in undrawn fibers are removed and amorphous chain are aligned. Finally, at DR4, recrystallization of aligned chains occurs, restoring crystallinity to approximately 70 %.

At DR1 fibers are highly crystalline, but the amorphous dichroic ratio favors parallel alignment while the crystalline favors perpendicular alignment to the axis. These opposing alignments indicate more disorder in macromolecular structure. At DR2, decrease in crystallinity with increase in both the crystalline and amorphous dichroic ratio illustrate the unfolding of lamella and realignment of amorphous chains and crystalline regions with draw. At DR3, the percent crystallinity continues to decrease, and the amorphous and crystalline dichroic ratio decreases to 1.8 and 0.4, respectively; indicating that crystalline structure has been further deformed. Finally, at DR4 the crystallinity increases to 71% and both dichroic ratios increase to values greater than 1. This appears to follow the accepted model of polymer crystal deformation, where initial crystal structures dislocate in the direction of applied strain, until amorphous chains are pulled out and aligned in the direction of draw. Chains continue to align under strain and recrystallize between extended chains in a fibrillar structure in the same manner as conventional drawing [33–35].

Crystal dislocation of PCL electrospun nanofiber during post-drawing likely occurs by screw dislocations in the lamellar [36]. PCL crystals grown from melts and solutions have been observed to form spherulitic structures, initiated by screw dislocations in the initial crystal lattice, and post-drawing will likely increase this effect in the structure of the crystal lattice (Fig. 6**A**) [8,37–39]. After the initial screw dislocation, lamellar structures continue to propagate off of the newly formed terrace in either direction resulting in the lamellar shapes sketched in Fig. 6**B**. These screw dislocations in the crystal lattice are likely the result of irregularly located carbonyl groups creating twist in the individual crystals, which would compound with nucleation [40]. As the crystal continues to nucleate, the crystal lattice branches, forming a hedrite (Fig. 6**C**) [41]. This process of crystal formation was further supported by observance of spherulites in PCL microfibers (Fig. 6**E**) [8]. In another study, AFM distinguished disordered lamellar structure in undrawn electrospun fibers, which appears to resemble the hedrite structures which form during initial formation of PCL spherulites (Fig. 6**D, F**) [42,43]. Although full spherulites may not form in the confined space of electrospun nanofibers, this evidence suggests crystal nucleation would initiate in the same manner. Therefore, hedrite structures with splayed crystal lattices likely form in the undrawn electrospun fiber and cause the lower dichroic ratios of the crystalline and amorphous regions (Fig. 5). In this case, as fibers are drawn, this screw dislocation of the crystal structure was likely encouraged, and able to proceed from any point in the crystal lattice where diverging crystalline arms occur. This would also explain the low strength, low chain orientation and high permeability of DR1 fibers.

Day 3 and Day 7: In PBS, fibers with high initial crystallinity, (DR1, DR4) lost crystallinity over time (Fig. 7**A**). A similar but opposite affect was observed for samples with lower initial crystallinity (DR2, 3). This effect has been seen for conventional fiber spinning, where stress applied to fibers during drawing and tensioning at crystallization temperatures can remove crystal structures if crystallinity was already high [44]. The dichroic ratios of the amorphous and crystalline regions of most samples were greater than 1 at D0 (favoring chain alignment parallel to the fiber axis) and decreased to values less than one at D7, which indicated a reduction in chain alignment parallel to the fiber axis and an increase in alignment perpendicular to the fiber axis (Fig. 7**B**). The dichroic ratio of the amorphous region (1157 cm^{-1}) of DR1 fluctuated over the incubation period, it first decreased at D3, then increased at D7, but remained below 1 indicating perpendicular chain alignment. The dichroic ratio of the amorphous region (1157 cm^{-1}) of DR2 continually decreased from 3.4 at D0 to 1.0 at D7, indicating a loss of anisotropic chain structure. The dichroic ratio of the crystalline region (1293 cm^{-1}) of DR3 did not change on D3, and increased on D7 but remained below 1, indicating perpendicular chain alignment. These fluctuations in both crystallinity and chain alignment illustrate that at the prescribed degradation conditions (37C, submerged) polymer chains are mobile despite high draw ratios and residual tension after tying to a 3D printed frame.

On D3, DR1 fibers in PBS increased in ultimate tensile strength by 172 %, while samples collected at different draw ratios did not change. This occurs despite the fact that prolonged exposure to liquid often reduces mechanical strength due to swelling as the surrounding media penetrates the material. It is possible that as the PBS penetrates the fiber, the hydrophobic nature of PCL causes the polymer chains to pack together rather than force them apart. The experiment temperature of 37 °C would allow the chains to recrystallize while the surrounding media forced the mobile chains together. This would result in a more densely packed crystalline structure at D3 than D0 and cause an increase in tensile strength despite a loss of chain alignment.

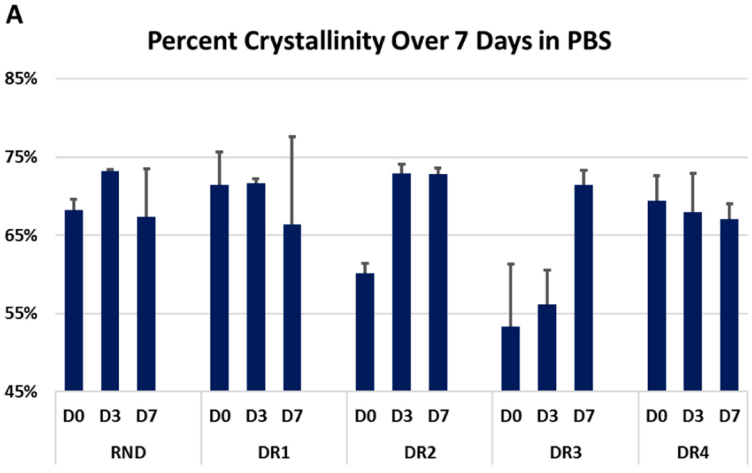

B

Dichroic Ratio Amorphous (1157cm^{-1})	DR1	DR2	DR3	DR4
D0	1.2	3.7	1.8	3.6
D3	0.23	1.9	1.1	1.2
D7	0.55	1.0	0.5	0.8

C

Dichroic Ratio Crystalline (1293cm^{-1})	DR1	DR2	DR3	DR4
D0	0.8	1.9	0.4	1.2
D3	0.4	1.2	0.4	1.1
D7	0.4	0.6	0.8	0.7

Fig. 6. (A) Changes in crystallinity and (B) chain alignment in the amorphous and crystalline regions of fiber collected at increasing draw ratio (DR), 1,2, 3, 4; submerged in PBS over 7 days.

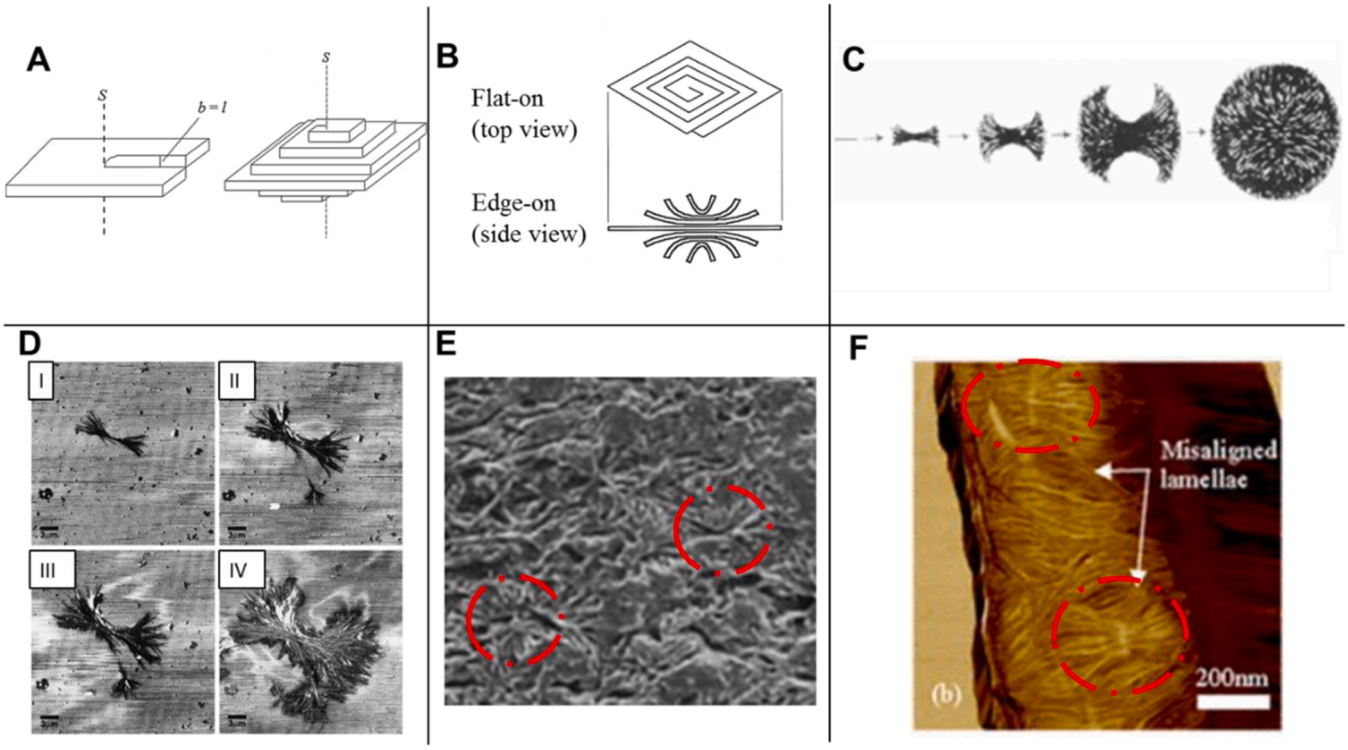

Fig. 7. Diagram of initiation of spherulite growth. A.) Diagram of screw dislocation of the initial lamella and propagation of crystal on newly formed terrace. B.) Diagram of crystal structure from flat-on (top-down view), and edge-on (side view). C.) Formation of spherulite from axialite to hedrite, to sheaf like structure to full spherulite in the edge on view [36,41]. Reproduced with permissions. Evidence for spherulitic growth in PCL prepared in different forms (D) initial progression of spherulite growth in PCL melt, hedrite, to sheaf formation (E) spherulite structures observed in undrawn PCL melt spun microfibers, (F) Hedrite structures in undrawn PCL electrospun fibers [8,42,43], reproduced with permissions.

When submerged in PS Lipase, DR2 and DR3 samples exhibit an increase in crystallinity over 7 days; at the same time, the alignment in the amorphous and crystalline regions fluctuates (Fig. 8**A–B**). In DR4, crystallinity was retained and similar changes to alignment are observed. The changes in alignment and loss of mass indicates that increased crystallinity results from a combination of lost amorphous chains from degradation by the lipase, as well as recrystallization.

DR1 pretension samples maintain percent crystallinity and dichroic ratios of the amorphous and crystalline regions over the 7-day degradation period (Fig. 9). The ability to maintain percent crystallinity combined with increased tensile strength and mass retention shows pretension likely acts as a secondary, continuous drawing phase. In this case, holding the tension over the degradation period improves chain alignment to the fiber axis, compacts chains together as diameter was reduced, and sets the chain structure in place similar to an annealing process [14,26].

This secondary stage continues to align chains to the fiber's axis (load direction), increasing strength after the initial draw during electrospinning and collection. The elevated temperature during degradation (37 °C), occurs above the glass transition temperature (– 60 °C)

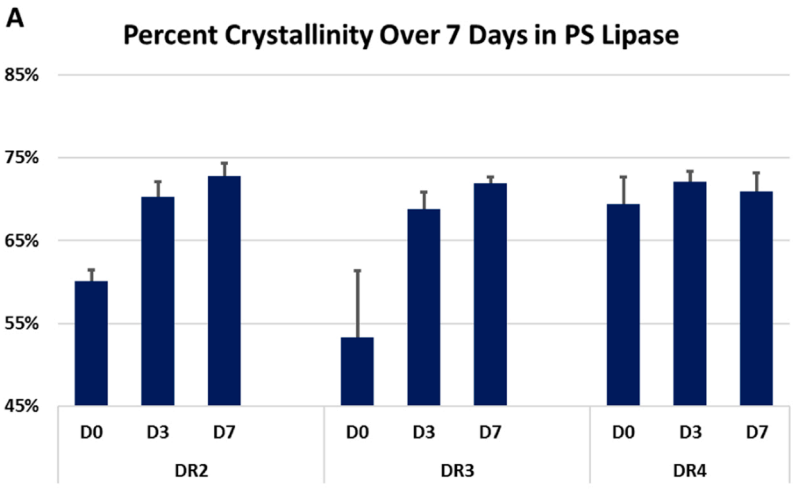

B

Dichroic Ratio Amorphous (1157cm^{-1})	DR2	DR3	DR4
D0	3.7	1.8	3.6
D3	0.4	0.6	0.7
D7	1.1	0.9	0.7

C

Dichroic Ratio Crystalline (1293cm^{-1})	DR2	DR3	DR4
D0	1.9	0.4	1.2
D3	0.3	0.4	0.5
D7	1	0.8	0.6

Fig. 8. (A) Changes in crystallinity and (B) chain alignment in the amorphous and crystalline regions of fiber collected at increasing draw ratio (DR), 1,2, 3, 4; submerged in PS Lipase over 7 days.

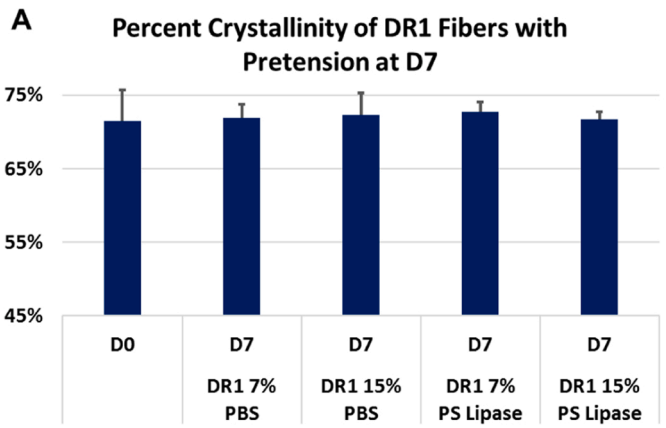

B

Dichroic Ratio Amorphous (1157cm^{-1})				
	DR1 7% PBS	DR1 15% PBS	DR1 7% PS Lipase	DR 15% PS Lipase
D0	1.2			
D7	1.5	1	3.3	0.5

C

Dichroic Ratio Crystalline (1293cm^{-1})				
	DR1 7% PBS	DR1 15% PBS	DR1 7% PS Lipase	DR 15% PS Lipase
D0	0.8			
D7	1.1	0.7	2.7	0.5

Fig. 9. (A) Changes in crystallinity and (B) chain alignment in the amorphous and crystalline regions of fiber collected at DR1 and pretension to 7 % and 15 % their maximum load, submerged in PBS and PS Lipase over 7 days.

increasing the ability of polymer chains to dislocate and rearrange in the direction of the applied pretension. Furthermore, because the process takes place below the melt-temperature (60 °C), crystal structures formed during initial drawing are not lost due to melting. Finally, because the process takes place within the PCL melt crystallization range (34–44 °C), new crystals form and align along the fiber axis in the direction of the pretension [38]. The formation of new crystals competes with the enzymatic degradation of crystals, resulting in the retention of 70 % crystallinity and a 2.2–3.8 × increase in ultimate tensile strength despite mass loss over the 7-day period.

In summary, collection and drawing cause initial polymer chain alignment and crystallinity in nanofiber samples. The elevated temperature during degradation increases chain mobility and without tension may result in a loss of chain alignment to the fiber axis, increase isotropic chain formation and increase spacing between amorphous chains, allowing faster penetration of enzyme and hydrolysis of polymer ester bonds. When fixation or pretension was applied, chains mobilized by increased temperature continue to align with the direction of the load applied along the fiber axis, resisting chain relaxation to isotropic structures. Because the tension was maintained for the duration of the degradation period at an elevated temperature, the polymer chains are able to form new crystals and align along the fiber axis. This illustrates the critical importance of pretensioning or appropriately annealing a material in order improve and retain macromolecular structure and by extension, increase and maintain tensile strength [26,44].

4. Conclusions

The automated track design successfully demonstrated the simultaneous collection and drawing of electrospun nanofibers in a continuous manufacturing process. Mechanical testing revealed that the tensile strength and Young's modulus increased systematically with draw. The ultimate tensile strength and Young's modulus are comparable or exceed that of other PCL microfibers and electrospun nanofibers in literature. End fixation and pretensioning fibers in order to keep the material in continuous tension during enzyme exposure was critical to retaining electrospun fiber material properties. Maintaining tension during enzyme exposure facilitates improving polymer chain alignment to the fiber axis, tensile strength, and crystallinity after collection. As a result, the degradation rate of the fibers is reduced.

Comparing mechanical strength, crystallinity, and chain orientation at D0 shows that tensile strength was highly dependent on chain alignment to the axis and can potentially be increased independent of fiber crystallinity (DR3). Meshes and bundles composed of fibers drawn to different ratios would likely be able to provide strong tensile strength and controllable degradation rate. The data presented showed that rate of degradation was highly dependent on both crystallinity and macromolecular orientation, which can be modified by automated track drawing.

Declaration of Competing Interest

The authors declare the following financial interests/personal relationships which may be considered as potential competing interests: Vince Beachley has patent pending to Rowan University.

Data Availability

Selected data is accessible in Mendeley Data: 10.17632/wsctdsdxpc.1.

Acknowledgements

Research was sponsored by the National Science Foundation (NSF1653329) and the Army Research Laboratory under Cooperative Agreement no. W911NF-17-2-0227. The views and conclusions contained in this document are those of the authors and should not be interpreted as representing the official policies, either expressed or implied, of the Army Research Laboratory or the U.S. Government. The U.S. Government is authorized to reproduce and distribute reprints for Government purposes not withstanding any copyright notation herein.

Appendix A. Supporting information

Supplementary data associated with this article can be found in the online version at doi:10.1016/j.mtcomm.2022.104990.

References

[1] J.-H. He, Y. Liu, L.-F. Mo, Y. Wan, L. Xu, Electrospun Nanofibres and Their Applications, 2008.
[2] Y. Gogotsi, Nanomaterials Handbook, CRC press, 2006.
[3] J. Yao, C. Bastiaansen, T. Peijs, High strength and high modulus electrospun nanofibers, Fibers 2 (2) (2014) 158–186.
[4] S. Ramakrishna, K. Fujihara, W.-E. Teo, T. Yong, Z. Ma, R. Ramaseshan, Electrospun nanofibers: solving global issues, Mater. Today 9 (3) (2006) 40–50.
[5] Z.-M. Huang, Y.Z. Zhang, M. Kotaki, S. Ramakrishna, A review on polymer nanofibers by electrospinning and their applications in nanocomposites, Compos. Sci. Technol. 63 (15) (2003) 2223–2253.
[6] J. Zeng, X. Chen, Q. Liang, X. Xu, X. Jing, Enzymatic degradation of poly(L-lactide) and poly(ε-caprolactone) electrospun fibers, Macromol. Biosci. 4 (12) (2004) 1118–1125.
[7] M.A. Woodruff, D.W. Hutmacher, The return of a forgotten polymer—polycaprolactone in the 21st century, Prog. Polym. Sci. 35 (10) (2010) 1217–1256.
[8] M. Mochizuki, M. Hirano, Y. Kanmuri, K. Kudo, Y. Tokiwa, Hydrolysis of polycaprolactone fibers by lipase: effects of draw ratio on enzymatic degradation, J. Appl. Polym. Sci. 55 (2) (1995) 289–296.

[9] T. Hayashi, H. Kanai, T. Hayashi, Enzymatic degradation of poly (ε-caprolactone) fibers in vitro, Polym. J. 33 (1) (2001) 38.
[10] R. Fields, F. Rodriguez, R. Finn, Microbial degradation of polyesters: polycaprolactone degraded by P. pullulans, J. Appl. Polym. Sci. 18 (12) (1974) 3571–3579.
[11] I. Castilla-Cortázar, J. Más-Estellés, J.M. Meseguer-Dueñas, J.L. Escobar Ivirico, B. Marí, A. Vidaurre, Hydrolytic and enzymatic degradation of a poly (ε-caprolactone) network, Polym. Degrad. Stab. 97 (8) (2012) 1241–1248.
[12] Z. Gan, Q. Liang, J. Zhang, X. Jing, Enzymatic degradation of poly (ε-caprolactone) film in phosphate buffer solution containing lipases, Polym. Degrad. Stab. 56 (2) (1997) 209–213.
[13] A. Vieira, J. Vieira, J. Ferra, F. Magalhães, R. Guedes, A. Marques, Mechanical study of PLA–PCL fibers during in vitro degradation, J. Mech. Behav. Biomed. Mater. 4 (3) (2011) 451–460.
[14] T.A. Osswald, G. Menges, Materials Science of Polymers for Engineers, Carl Hanser Verlag GmbH Co KG, 2012.
[15] C.X. Lam, M.M. Savalani, S.-H. Teoh, D.W. Hutmacher, Dynamics of in vitro polymer degradation of polycaprolactone-based scaffolds: accelerated versus simulated physiological conditions, Biomed. Mater. 3 (3) (2008), 034108.
[16] W.J. Cook, J.A. Cameron, J.P. Bell, S.J. Huang, Scanning electron microscopic visualization of biodegradation of polycaprolactones by fungi, J. Polym. Sci.: Polym. Lett. Ed. 19 (4) (1981) 159–165.
[17] Z. Gan, J.T. Fung, X. Jing, C. Wu, W. Kuliche, A novel laser light-scattering study of enzymatic biodegradation of poly (ε-caprolactone) nanoparticles, Polymer 40 (8) (1999) 1961–1967.
[18] D.A. Brennan, D. Jao, M.C. Siracusa, A.R. Wilkinson, X. Hu, V.Z. Beachley, Concurrent collection and post-drawing of individual electrospun polymer nanofibers to enhance macromolecular alignment and mechanical properties, Polymer 103 (2016) 243–250.
[19] R.F. Edlich, Surgical Knot Tying Manual, Covidien, 2008.
[20] R. Ma, M. Schaer, T. Chen, J. Nguyen, C. Voigt, X.-H. Deng, S.A. Rodeo, The effects of tensioning of the anterior cruciate ligament graft on healing after soft tissue reconstruction, J. Knee Surg. (2019).
[21] ASTM C1557-20 STMfTSaYsMoF, ASTM International, West Conshohocken, PA, 2020.
[22] Y. He, Y. Inoue, Novel FTIR method for determining the crystallinity of poly (ε-caprolactone), Polym. Int. 49 (6) (2000) 623–626.
[23] X. Wang, H. Zhao, L.-S. Turng, Q. Li, Crystalline morphology of electrospun poly (ε-caprolactone) (PCL) nanofibers, Ind. Eng. Chem. Res. 52 (13) (2013) 4939–4949.
[24] T. Elzein, M. Nasser-Eddine, C. Delaite, S. Bistac, P. Dumas, FTIR study of polycaprolactone chain organization at interfaces, J. Colloid Interface Sci. 273 (2) (2004) 381–387.
[25] M. Coleman, J. Zarian, Fourier-transform infrared studies of polymer blends. II. Poly (ε-caprolactone)–poly (vinyl chloride) system, J. Polym. Sci.: Polym. Phys. Ed. 17 (5) (1979) 837–850.
[26] W.D. Callister, Materials Science and Engineering: An Introduction, John Wiley, 2007.
[27] Z. Gan, D. Yu, Z. Zhong, Q. Liang, X. Jing, Enzymatic degradation of poly (ε-caprolactone)/poly(dl-lactide) blends in phosphate buffer solution, Polymer 40 (10) (1999) 2859–2862.
[28] M.R. Williamson, Gravity spun polycaprolactone fibers for applications in vascular tissue engineering: proliferation and function of human vascular endothelial cells, Tissue Eng. 12 (1) (2006).
[29] A. Gurarslan, Y. Caydamli, J. Shen, S. Tse, M. Yetukuri, A.E. Tonelli, Coalesced poly(epsilon-caprolactone) fibers are stronger, Biomacromolecules 16 (3) (2015) 890–893.
[30] H.A. McKenna, J.W. Hearle, N. O'Hear, Handbook of Fibre Rope Technology, Elsevier, 2004.
[31] D. Kołbuk, P. Sajkiewicz, T.A. Kowalewski, Optical birefringence and molecular orientation of electrospun polycaprolactone fibers by polarizing-interference microscopy, Eur. Polym. J. 48 (2) (2012) 275–283.
[32] T. Hayashi, K. Nakayama, M. Mochizuki, T. Masuda, Studies on biodegradable poly (hexano-6-lactone) fibers. Part 3. Enzymatic degradation in vitro (IUPAC Technical Report), Pure Appl. Chem. 74 (5) (2002) 869–880.
[33] Z.K. Walczak, Formation of synthetic fibers, 1977.
[34] R. Young, P. Lovell, Introduction to Polymers, 2011.
[35] T. Matsumoto, T. Kawai, H. Maeda, Molecular unfolding in the drawing process of polyethylene films, Die Makromol. Chem.: Macromol. Chem. Phys. 107 (1) (1967) 250–252.
[36] B. Crist, J.M. Schultz, Polymer spherulites: a critical review, Prog. Polym. Sci. 56 (2016) 1–63.
[37] D. Bassett, Ciliation and Lamellae in Crystalline Polymers, Wiley Online Library, 1997, pp. 121–126.
[38] V. Speranza, A. Sorrentino, F. De Santis, R. Pantani, Characterization of the polycaprolactone melt crystallization: complementary optical microscopy, DSC, and AFM studies, ScientificWorldJournal 2014 (2014), 720157.
[39] H.F. Brinson, L.C. Brinson, Polymer engineering science and viscoelasticity. An introduction, 2008.
[40] Y. Chatani, Y. Okita, H. Tadokoro, Y. Yamashita, Structural studies of polyesters. III. Crystal structure of poly-ε-caprolactone, Polym. J. 1 (5) (1970) 555–562.
[41] L. Gránásy, T. Pusztai, T. Börzsönyi, G. Toth, G. Tegze, J. Warren, J. Douglas, Polycrystalline patterns in far-from-equilibrium freezing: a phase field study, Philos. Mag. 86 (24) (2006) 3757–3778.
[42] L. Beekmans, G.J. Vancso, Real-time crystallization study of poly (ε-caprolactone) by hot-stage atomic force microscopy, Polymer 41 (25) (2000) 8975–8981.
[43] C. Lim, E. Tan, S. Ng, Effects of crystalline morphology on the tensile properties of electrospun polymer nanofibers, Appl. Phys. Lett. 92 (14) (2008), 141908.
[44] Z.K. Walczak, Processes of Fiber Formation, Elsevier, 2002.